Analysis of plasma detachment in the magnetic thrust chamber using full particle-in-cell simulation

Kojima, Tomihiko
Interdisciplinary Graduate School of Engineering Sciences, Kyushu University

Morita, Taichi
Faculty of Engineering Science, Kyushu University

Yamamoto, Naoji
Faculty of Engineering Science, Kyushu University

出版情報：High Energy Density Physics. 36 (100814), 2020-08. Elsevier
バージョン：
権利関係：

Analysis of plasma detachment in the magnetic thrust chamber using full particle-in-cell simulation

Tomihiko Kojima[a,*], Taichi Morita[b] and Naoji Yamamoto[b]

[a]Interdisciplinary Graduate School of Engineering Sciences, Kyushu University, Kasuga 816-8580, Japan
[b]Faculty of Engineering Sciences, Kyushu University, Kasuga 816-8580, Japan

ARTICLE INFO

Keywords:
Magnetic nozzle
Magnetic Thrust Chamber
Plasma detachment
Particle-in-cell

ABSTRACT

A magnetic nozzle, which is a convergent-divergent magnetic field to control a plasma flow, has been investigated for application to plasma propulsion systems in spaceships. In the magnetic nozzle, plasma thermal energy is converted to one-directional kinetic energy by Lorentz force to generate thrust. Although magnetic field structure and strength are optimized for improvement of the thrust performance, it is essential to understand physical processes of plasma ejection from the nozzle, because the plasma may flow back along lines of magnetic field if the directed plasma continues being strongly magnetized. It is assumed, for one of the scenarios to explain a plasma detachment, that a plasma detaches from magnetic field when a cyclotron radius exceeds a scale length of magnetic field in size. Hence, we investigate a plasma detachment condition by analyzing parameters of the plasma for unmagnetization. We assumed individual particle motion of a fully ionized plasma in the magnetic nozzle and conducted a full particle-in-cell simulation in a two-dimensional coordinate system. We calculated a ratio of cyclotron radius to a scale length of the magnetic field. The ratio increased in a downstream due to variation of magnetic field induced from a diamagnetic cavity, suggesting unmagnetization.

1. Introduction

In the space propulsion study, a magnetic nozzle has been investigated to be applied to advanced propulsion systems such as a Magneto-Plasma-Dynamic thruster [1, 2], a Helicon plasma thruster [3], and VASIMR [4]. The system is equipped with a coil or magnet at an outlet of the thruster, which generates convergent-divergent magnetic field, and an induced plasma in the magnetic field is converted to an axial plasma flow on cylindrical coordinates by Lorentz force, $\boldsymbol{J} \times \boldsymbol{B}$, where $\boldsymbol{J}$ is a diamagnetic current in an azimuth direction. The coil or magnet is noncollisional with the plasma, therefore, the magnetic nozzle is expected to prolong the total lifetime of a thruster. Figure 1 shows thrust generation mechanism via Lorentz force. First, an initial plasma is generated in the external convergent-divergent magnetic field generated by the electromagnetic coil, and the plasma expands spherically. When the plasma expands adiabatically and velocity distribution is Maxwellian, fastest charged particles locate at an expansion radius of plasma and slower charged particles locate at an inner part of plasma, and there is a gradient of plasma number density. An outer product of $\boldsymbol{B}_z$ and the gradient of plasma number density causes a diamagnetic current on the expansion surface of plasma. Second, an induced diamagnetic current in the plasma, $\boldsymbol{J}$, and the external magnetic field, $\boldsymbol{B}$ generate the Lorentz force: $\boldsymbol{J} \times \boldsymbol{B}$, and it converts a plasma flow velocity in the positive z direction in Fig. 1. As a reaction force, the coil obtains thrust.

We have investigated a space propulsion system which ejects high-energy plasma such as an inertial fusion plasma by Lorentz force. This system is called a magnetic thrust chamber [5, 6, 7, 8, 9]. The magnetic thrust chamber expels the plasma as an unsteady flow. This thruster varies a repetition frequency of thrust generation. The magnetic thrust chamber can handle a fusion plasma for a laser fusion rocket (LFR) [10, 11, 12, 13]. Maeno *et al.* have directly measured the impulse of the magnetic thrust chamber [14]. Although they have proven that the magnetic thrust chamber generates thrust, there are still unsolved issues.

One of the issues is whether a plasma detaches from the magnetic field after the plasma flow velocity is converted in the axial direction. When the directed plasma contin-

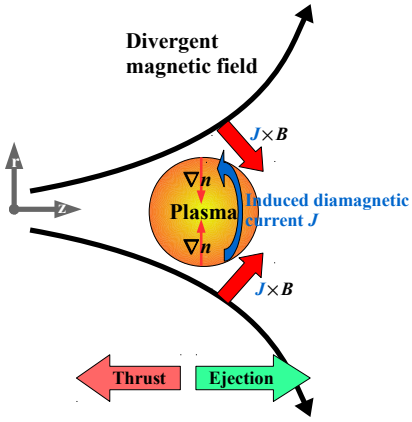

Figure 1: Thrust generation mechanism in the external divergent magnetic field. An initial plasma is generated in the magnetic field and expands spherically. An induced diamagnetic current in the plasma and the magnetic field generate Lorentz force, $\boldsymbol{J} \times \boldsymbol{B}$, and the plasma is directed to the positive z direction. As a reaction force, the coil is accelerated in the negative z direction.

*Corresponding author
t.kojima.500@s.kyushu-u.ac.jp (T. Kojima)
ORCID(s):

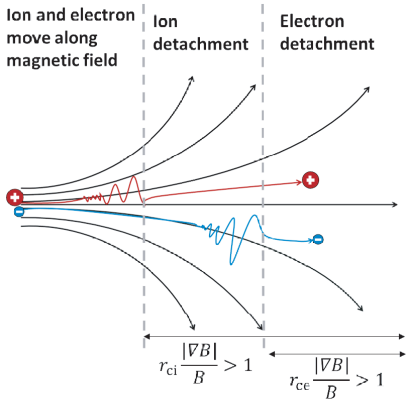

Figure 2: Plasma detachment due to increase in cyclotron radius. Ions detach from magnetic field earlier because r_{ci} is much larger than r_{ce}. If electrons also detach from magnetic field, the plasma is successfully ejected with charge neutrality.

ues being magnetized in the convergent-divergent magnetic field, the plasma may travel along the looped lines of magnetic field and thrust gain decreases. Electrons are trapped in magnetic field more strongly than ions due to the difference of cyclotron radius: $r_c \propto m$, where m is the mass of ion or electron. Several studies agree that ion deviates from the divergent magnetic field, when $f_{ci}L_B/V_i$ becomes order of unity, where f_{ci}, L_B, and V_i are ion cyclotron frequency, characteristic scale length of magnetic field inhomogeneity: $L_B = B/|\nabla B|$, and ion flow velocity, respectively [15, 16, 17, 18]. However, electron detachment has never been shown directly. If ions detach from magnetic field as same as the prior studies and electrons move along magnetic field, an electric field is induced by charge separation between the detached ions and electrons in the plasma. In such a situation, the ejected ions may return partially to the magnetic thrust chamber, and the thrust may decrease. Thrust performance of the magnetic thrust chamber has been estimated using a hybrid model simulation [19, 20], however, the charge separation has never been considered in these simulations, therefore, the effect of electric field on the plasma detachment is unclear. Hence, we will review the performance of the magnetic thrust chamber in terms of the detachment of ions and electrons.

One of the plasma detachment scenarios is that charged particles deviate from magnetic field where their cyclotron radii get extremely larger than the characteristic scale length of magnetic field gradient in a single cyclotron period: $r_c > L_B$ as shown in Fig. 2. The magnetic moment of charged particle may be not conserved in this condition, and the magnetic field barely holds the plasma. We investigated whether the above detachment scenario is applied to the magnetic thrust chamber using a full particle-in-cell (PIC) simulation, which is a first-principle method for collisionless plasma, and both ions and electrons are treated as individual superparticles. The initial condition of the plasma was determined to satisfy that the ratio of plasma kinetic energy to magnetic field energy is order of unity. Ion and electron cyclotron radii were compared with the characteristic scale length of magnetic field gradient. The results showed that electrons can be unmagnetized in the downstream of the system to detach from the magnetic field, where r_{ce}/L_B exceeds the unity.

2. Full PIC simulation

We conducted a full PIC simulation using the EPOCH [21, 22, 23] code to clarify the criterion of the plasma detachment. We applied a two-dimensional calculation model to allocate a sufficient number of calculation grids for a large area in the ejection direction. The grid width was smaller than the electron inertial length of initial expansion plasma, namely, $\Delta x = \Delta y = 0.1c/\omega_{pe}$, where c is the speed of light, and ω_{pe} is electron plasma frequency. The total number of calculation grids was expanded from 100×100, which was used in the calculation by Kawabuchi *et al.* [24], into 4000×4000 to simulate a plasma in a larger spatial scale in the downstream. The time step of calculation was determined by the Courant-Friedrichs-Lewy (CFL) condition, $\Delta t = \Delta x/c \sim 5 \times 10^{-16}$ s. The external magnetic field in the magnetic thrust chamber was induced by coil currents, which are located at $x = -0.45$ mm, and $y = \pm 0.15$ mm as shown in Fig. 3. Calculation parameters are listed in Table 1. R_C is the coil radius in the magnetic thrust chamber. The distance between coil currents is $2R_C$. The distance from the coil center to the center of initial plasma, L_C, is $3R_C$. r_{ci} and r_{ce} are ion and electron cyclotron radii, respectively, under the initial magnetic field. ε_b is a dimensionless parameter for the magnetic thrust chamber, defined as $\varepsilon_b = r_{ci}/R_b$ [24, 25], where R_b is defined as a plasma expansion radius in which magnetic field energy is comparable with an initial plasma kinetic energy, $R_b = \left(3\mu_0 E_0/\left(2\pi {B_0}^2\right)\right)^{1/3}$ [26, 27]. When the plasma is adequately magnetized: $\varepsilon_b \leq 1$, a diamagnetic current is generated in the plasma for thrust generation, and ε_b is one of the important parameters for the magnetic thrust chamber. The ratio of ion mass to electron mass, m_i/m_e, is 100 to calculate both ion and electron behavior in realistic calculation time. Initially, all particles were located in the plasma radius, R_p, to simulate an isotropically expanding plasma. The initial velocity of the particles was determined by their positions, $V_p = r_p V_0/R_p$, and the maximum velocity was defined at the plasma edge, $r_p = R_p$ as $V_0 = 141$ km/s. The initial ion and electron temperatures, T_i and T_e, were estimated to be zero, and the initial number densities of ion and electron, n_i and n_e were 10^{24} m^{-3} as same as the previous model [24]. The total number of super-particles was 1×10^6.

3. Simulation results

3.1. $J \times B$ generation in the magnetic thrust chamber

Figures 4(a)-(c) show the time evolution of the strength of magnetic field. Figure 4(a) shows the strength of magnetic field at 0.1 ns. There is almost no change from the initial magnetic field, because the initial plasma expansion near $(x, y) = (0,0)$ is small. The magnetic field is weakened in a

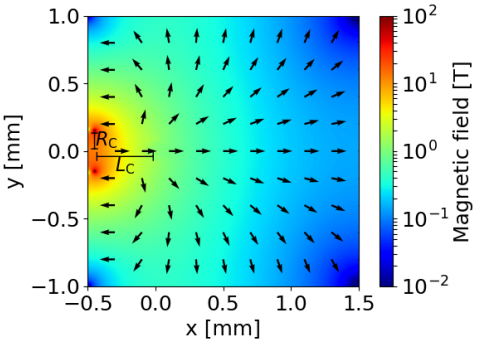

Figure 3: The structure of initial magnetic field. The coil currents in $\pm z$ direction are located at $x = -0.45$ mm, and $y = \pm 0.15$ mm.The initial plasma is located in a circle, where the center is $x = 0$ mm, and $y = 0$ mm. The radius, R_p , is 0.065 mm.

Table 1
Calculation parameters and initial condition of plasma

Parameters	
Number density	$n_i = n_e = 10^{24}$ m^{-3}
Electron inertial length	$c/\omega_{pe} \sim 5$ μm
Time-step	$\Delta t = 5.6 \times 10^{-16}$ s
Grid width	$\Delta x = 0.5$ μm
Coil radius	$R_C = 300\Delta x$
Coil position	$L_C/R_C = 3$
Ion cyclotron radius	$r_{ci}/R_C = 0.52$
Electron cyclotron radius	$r_{ce}/R_C = 0.0052$
$\varepsilon_b = r_{ci}/R_b$	1
Mass ratio	$m_i/m_e = 100$
Number of super-particles	1×10^6
Maximum particle speed	$V_0 = 141$ km/s (= 0.141 mm/ns)

plasma region at 0.5 ns as shown in Fig. 4(b) , because the diamagnetic current, J_z is induced in the plasma as shown in Fig. 4(d). In consequence, a diamagnetic cavity is generated at 1.5 ns as shown in Fig. 4(c). Figures 4(e) and (f) show x and y components of $J \times B$ at 0.5 ns, respectively. The $J \times B$ works to push back the plasma in the positive x direction. The thrust generation mechanism of the magnetic thrust chamber is satisfied in this calculation.

3.2. Time-variation of ion and electron flows

Figure 5 shows two-dimensional spatial distributions of ions and electrons at 0.5 ns [Figs. 5(a) and (b)] and 1.5 ns [Figs. 5(c) and (d)]. The red and blue plots show the ion and electron number densities, respectively. The black arrows in Fig. 5 show lines of magnetic field. As shown in Figs. 5(a) and (b), ions and electrons in $x > 0.2$ mm show lower number density ($\sim 10^{21}$ m^{-3}) because particles which have positive V_x in the initial plasma radius expand adiabatically toward a downstream. Ions and electrons in $x \leq 0.2$ mm show higher number density ($\gtrsim 10^{22}$ m^{-3}), forming a structure along the line of magnetic field. Because the plasma locates in $x < 0$ mm has negative V_x initially, and it interacts with a stronger

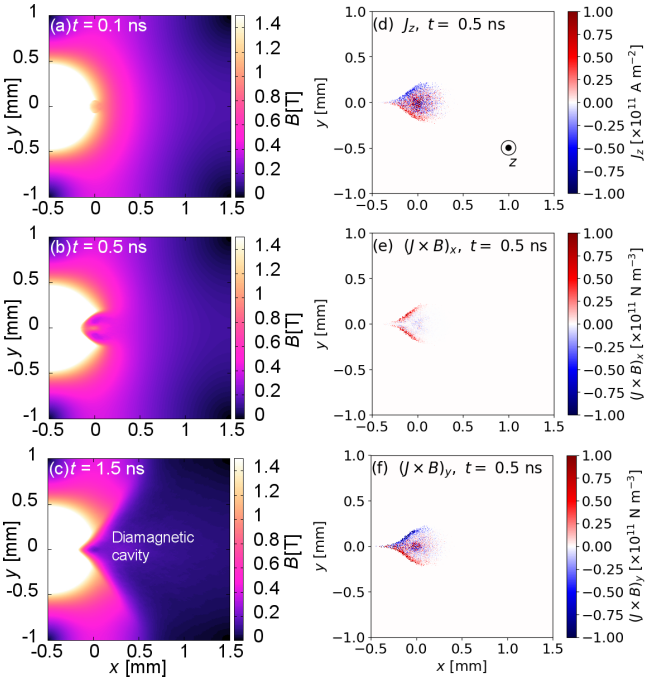

Figure 4: Magnetic flux density at t = (a)0.1 ns, (b)0.5 ns and (c)1.5 ns, respectively. (d)J_z, (e)x and (f)y components of $J \times B$ at 0.5 ns.

magnetic field in an upstream. Namely, the V_x is converted to V_y and V_z by the magnetic field, and V_x decreases, resulting in the increase of the number density. As shown in Figs. 5(c) and (d), $J \times B$ converts the momentum of plasma in the positive x direction, and most of ions and electrons move in the positive x direction.

Figure 6 shows flow vectors of ion (red) and electron (blue) with magnetic field vectors (black) at 1.5 ns in the regions of (a)0.3 mm $\leq x \leq$ 0.5 mm, and 0.5 mm $\leq y \leq$ 0.7 mm and (b)0.7 mm $\leq x \leq$ 0.9 mm, and 0.6 mm $\leq y \leq$ 0.8 mm as shown in Figs. 5(c) and (d). The region (a) was selected as the stronger magnetic field region, and the region (b) was selected as the lower limit region where the flow vector is computable in the downstream, representatively. The difference between the flow vector and the magnetic field vector at each location was compared in the two magnetic field conditions.

In the region (a), ion and electron flow vectors are parallel to the magnetic field vectors, and both particles move together along the magnetic field. No plasma detaches from the magnetic field in this region. On the other hand, in the region (b), ion and electron flow vectors are non-parallel to a magnetic field vector, indicating a possibility of the detachment. It is needed to analyze magnetized parameters of plasma in the downstream to understand the detachment parameters.

3.3. Time-variation of ion and electron cyclotron radii

Figure 7 shows ion number density at t = (a)0.5 ns, (b)1.0 ns, (c)1.5 ns, and (d)2.0 ns, and ion cyclotron radius, elec-

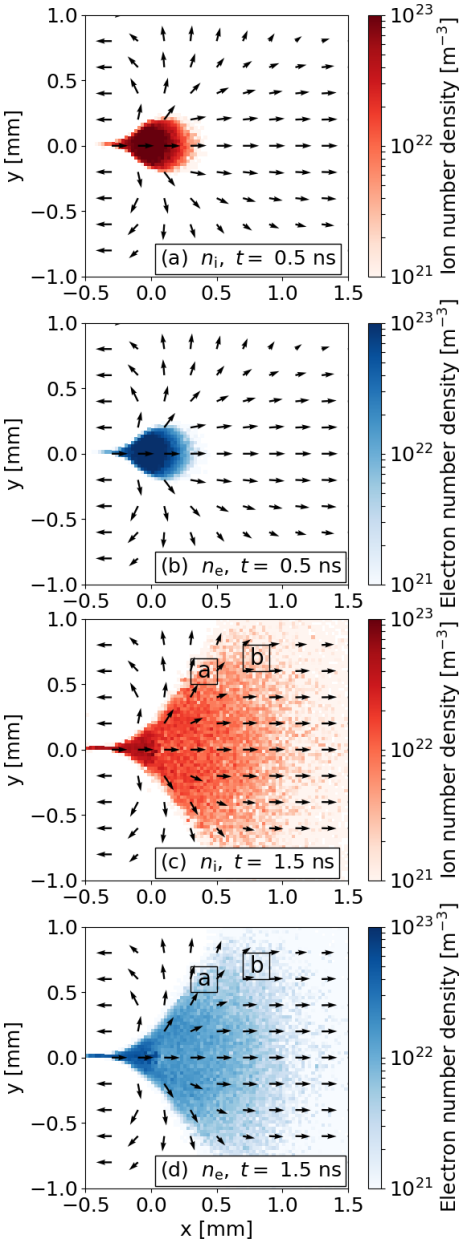

Figure 5: Ion number density at t = (a)0.5 ns and (c)1.5 ns, and electron number density at t = (b)0.5 ns and (d)1.5 ns in the magnetic field, respectively. Black arrows show lines of magnetic field.

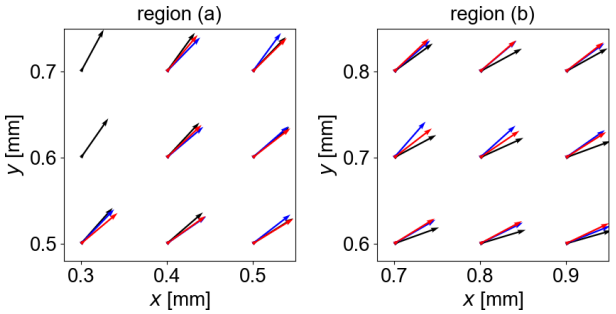

Figure 6: Flow vectors of ion (red) and electron (blue). Black arrows show lines of magnetic field. Ion and electron move along magnetic field at the region (a). Ion and electron show deviation from lines of magnetic field at the region (b).

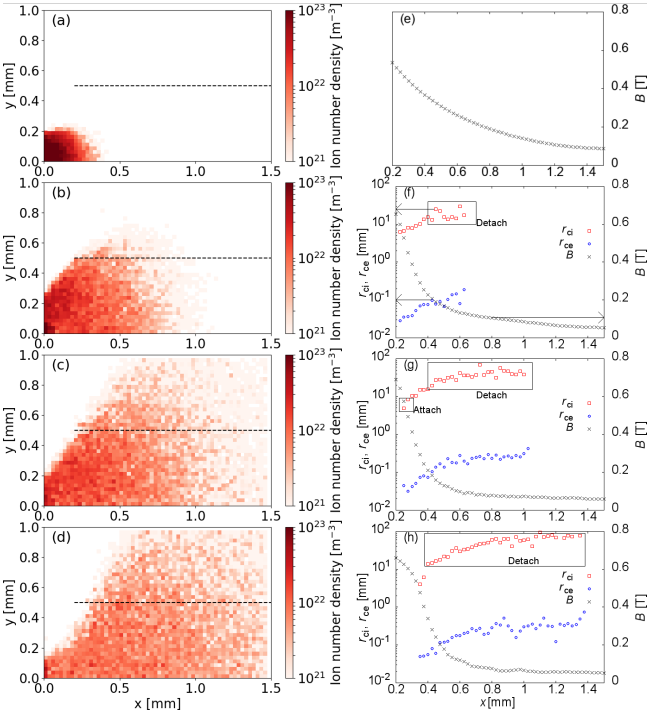

Figure 7: Ion number density at t = (a)0.5 ns,(b)1.0 ns, (c)1.5 ns, and (d)2.0 ns. Ion and electron cyclotron radii and magnetic flux density at y = 0.5 mm at t = (e)0.5 ns,(f)1.0 ns, (g)1.5 ns, and (h)2.0 ns. r_{ci} and r_{ce} increase in the downstream. r_{ci} exceeds the plasma expansion radius ($L \sim 1$ mm), and ions detach from the magnetic field.

tron cyclotron radius, and absolute value of magnetic flux density in (0.2 mm $\leq x \leq$ 1.5 mm , y = 0.5 mm) at (e)0.5 ns, (f)1.0 ns, (g)1.5 ns, and (h)2.0 ns. The definition of cyclotron radius is V_{Th}/ω_c, where V_{Th} is thermal velocity and ω_c is cyclotron frequency. In the present calculation, a number of super-particles in one cell is small in a low density region. Therefore, V_{Th} is calculated from Gaussian fitting of $V_{\perp B}$ distribution in $50\Delta x \times 50\Delta y$ region, where $V_{\perp B}$ is a perpendicular velocity of each super-particle to a magnetic field vector. Figure 7(e) shows only B, meaning the plasma expansion radius is smaller than 0.5 mm at 0.5 ns as shown in Fig. 7(a), and the distribution of magnetic flux density is same as the initial magnetic field. As shown in Fig. 7(b), ions and electrons expand and reach y = 0.5 mm at 1.0 ns. As shown in Fig. 7(f), the magnetic flux density decreases by 60-70 % compared with initial values at 0.2 mm $< x <$ 0.8 mm due to the diamagnetism of the plasma. r_{ci} exceeds 10 mm which is ten times larger than the plasma expansion radius, $L \sim$ 1 mm, as shown in Fig. 5. Therefore, ions are unmagnetized at $x >$ 0.4 mm. On the other hand, r_{ce} is less than 1 mm, meaning that the electrons are magnetized ($r_{ce} \ll L$) in 0.2 mm $< x <$ 0.4 mm, and weakly magnetized ($r_{ce} \lesssim L$) in $x \geq$ 0.4 mm. As shown in Fig. 7(c)

and (g), ions and electrons continue expanding to positive x direction at 1.5 ns. Ions are unmagnetized and electrons are weakly magnetized ($r_{ci} \gg L$ and $r_{ce} < L$) in $x \geq 0.5$ mm. As shown in Fig. 7(d) and (h), ions and electrons continue expanding in the downstream at 2.0 ns. r_{ci} increases as going to the downstream because the magnetic flux density decreases in the downstream. Ions are unmagnetized at $x > 0.4$ mm, and r_{ci} keeps increasing. Therefore, ions detach from magnetic field. On the other hand, a spatial difference of r_{ce} is unsteady at $x > 0.8$ mm, and it is unclear that r_{ce} increases in the downstream. It is difficult to discuss electron detachment only from the value of r_{ce}.

3.4. Evaluation of electron detachment

It is insufficient to evaluate an electron detachment by comparing r_{ce} with the plasma expansion radius, thus, r_{ce} is compared with smaller characteristic scale length, L_B. Figure 8 shows the spatial distribution of r_{ce}/L_B at each calculation time. The value of r_{ce}/L_B increased with electron expansion to the downstream because the magnetic flux density decreases and, r_{ce} becomes larger as shown in Fig. 7. As shown in Figs. 8(b) and (c), the value exceeds the order of unity in $x \geq 0.5$ mm, indicating that there is a boundary of the ratio r_{ce}/L_B at $x \sim 0.5$ mm. Figure 9 shows the comparison of cyclotron radii between normalized by L and L_B. L and L_B are computed at the time of the observation. L_B is computed at each location. r_{ce}/L_B is larger than each r_{ce}/L because L_B includes the spatial variation of magnetic field. It indicates that r_{ce}/L_B is a better parameter to evaluate the electron detachment. The increase of r_{ce}/L_B is correlation with the magnetic moment of charged particle, $\mu_p \propto {V_{\perp B}}^2/B$. When μ_p is conserved in a magnetic field which has a gradient, the charged particle attaches to the line of magnetic field. Although μ_p is almost constant in the strong magnetic field region ($x \leq 0$), it increases more than ten times from that of the initial condition in a downstream($x > 0$) in the simulation. This indicates a violation of μ_p conservation in the downstream, and it is clarified by the generation of the diamagnetic cavity because of $\mu_p \propto 1/B$. In the condition, the magnetic field barely holds the plasma, and the plasma deviates from the magnetic field.

The plasma reaches the calculation boundary at 2.0 ns, and the outer electromagnetic field condition later in time is obscure in the present calculation. The value of r_{ce}/L_B will keep increasing in a downstream.

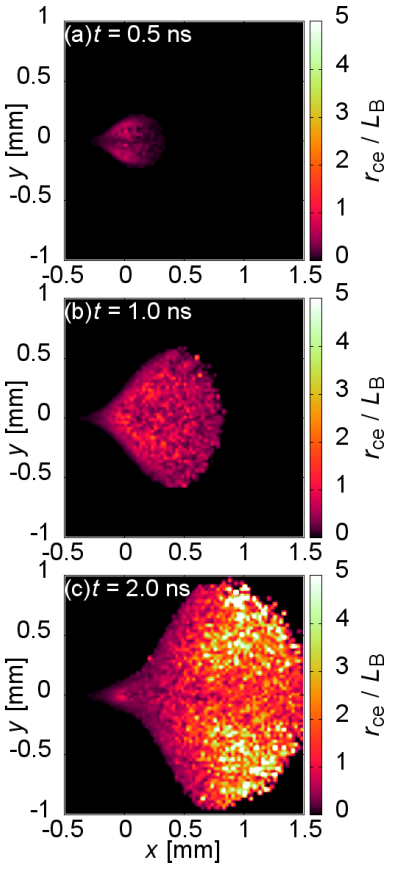

Figure 8: Electron cyclotron radius over the characteristic scale length of magnetic field gradients, r_{ce}/L_B. $r_{ce}/L_B \leq 1$ shows the attachment to the magnetic field, and $r_{ce}/L_B \gg 1$ is detachment.

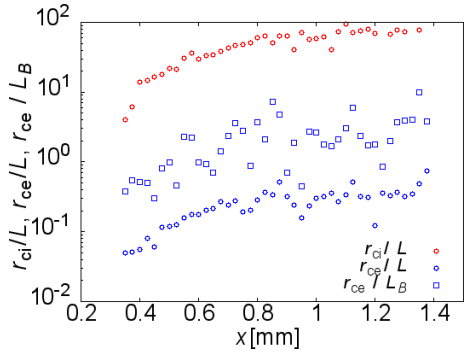

Figure 9: Ion and electron cyclotron radii over the plasma expansion radius, and r_{ce}/L_B at $y = 0.5$ mm at $t = 2.0$ ns.

4. Conclusion

We have analyzed plasma flow in a magnetic thrust chamber in the case of the ratio of the plasma kinetic energy to the magnetic field energy is unity. The analyzed ion and electron cyclotron radii showed unmagnetized ions and weakly magnetized electrons. It is found that ions detach from magnetic field in the downstream. Furthermore, we have discussed the evaluation method of electron detachment using the relationship between the cyclotron radius and the characteristic scale length of magnetic field gradients. A boundary was found in the plasma where r_{ce}/L_B exceeded the order of unity in the downstream. A diamagnetic cavity is found in the plasma region, and μ_p increased extremely. We considered that the violation of μ_p conservation induces the electron detachment in the calculation. Electron detachment will be clarified when we investigate the critical condition of detachment analyzing the downstream farther from the coil.

Acknowledgment

The computations were performed using the Research Institute for Information Technology (Kyushu University). This research was partially supported by JSPS KAKENHI grant number 17K14876.

References

[1] H. Nabuchi, K. Suzuki, Y. Kobayashi, A. Komuro, K. Takahashi, A. Ando, Thrust enhanced by a magnetic laval nozzle in an applied-field magneto-plasma-dynamic thruster, Plasma and Fusion Research 11 (2016) 2406033–2406033.

[2] M. Coletti, Simple thrust formula for an mpd thruster with applied-magnetic field from magnetic stress tensor, 2007.

[3] F. N. Gesto, B. D. Blackwell, C. Charles, R. W. Boswell, Ion detachment in the helicon double-layer thruster exhaust beam, Journal of Propulsion and Power 22 (2006).

[4] A. Ilin, F. DÃŋaz, J. Squire, A. Tarditi, B. Breizman, M. Carter, Simulation of plasma detachment in vasimr, 2002. doi:10.2514/6.2002-346.

[5] Y. Nagamine, H. Nakashima, Analysis of plasma behavior in a magnetic thrust chamber of a laser fusion rocket, Fusion Science and Technology 35 (1999) 62–70.

[6] K. V. Vchivkov, H. Nakashima, F. Ichikawa, Y. P. Zakharov, Optimization of thrust efficiency in laser fusion rocket by using three-dimensional hybrid particle-in-cell code, Vacuum 73 (2004) 427–432.

[7] A. Maeno, A. Sunahara, S. Fujioka, H. Nakashima, Effect of magnetic field strength on a magnetic thrust chamber system, Journal of Propulsion and Power 30 (2014) 54–61.

[8] F. Morita, M. Edamoto, S. Miura, A. Sunahara, N. Saito, Y. Itadani, T. Kojima, Y. Mori, T. Johzaki, Y. Kajimura, S. Fujioka, A. Yogo, H. Nishimura, H. Nakashima, N. Yamamoto, Control of unsteady laser-produced plasma-fow with a multiple-coil magnetic nozzle, Journal of Propulsion and Power 7 (2017).

[9] N. Saito, N. Yamamoto, T. Morita, M. Edamoto, H. Nakashima, S. Fujioka, A. Yogo, H. Nishimura, A. Sunahara, Y. Mori, T. Johzaki, Experimental demonstration of ion extraction from magnetic thrust chamber for laser fusion rocket, Japanese Journal of Applied Physics 57 (2014).

[10] R. Hyde, L. Wood, J. Nuckolls, Prospects for rocket propulsion with laser-induced fusion microexplosions, AIAA/SAE 8th Joint Propulsion Specialist Conference (1972).

[11] C. D. Orth, G. Klein, J. Sercel, N. Hoffman, K. Hurray, F. Chang-Diaz, The vista spacecraft–advantages of icf for interplanetary fusion propulsion applications, UCRL-96676 Preprint, IEEE 12th Symposium on Fusion Engineering (1987).

[12] H. Nakashima, H. Shoyama, Y. Kanda, Y. Nakano, Parametric design study of laser fusion rocket, in: the 18th International Symposium on Space Technology and Science, volume 1 & 2, 1992, pp. 19–24.

[13] H. Nakashima, Y. Kajimura, Y. Kozaki, Y. P. Zakharov, A laser fusion based on fast ignition concept, in: the 56th International Astronautical Congress, 2005.

[14] A. Maeno, N. Yamamoto, H. Nakashima, S. Fujioka, T. Johzaki, Y. Mori, A. Sunahara, Direct measurement of the impulse in a magnetic thrust chamber system for laser fusion rocket, Applied Physics Letters 99 (2011).

[15] K. Terasaka, S. Yoshimura, K. Ogiwara, M. Aramaki, M. Y. Tanaka, Experimental studies on ion acceleration and stream line detachment in a diverging field, Physics of Plasmas 17 (2010).

[16] K. Terasaka, S. Yoshimura, K. Ogiwara, M. Aramaki, M. Y. Tanaka, Observation of ion stream line detachment and onset of azimuthal rotation in a diverging magnetic field, IEEE Transactions on Plasma Science 39 (2011) 2470–2471.

[17] M. D. Carter, F. R. Chang-DÃŋaz, A. V. Ilin, D. O. Sparks, Radio frequency plasma applications for space propulsion, in: International Conference on Electromagnetics in Advanced Applications, 1999.

[18] C. S. Olsen, M. G. Ballenger, M. D. Carter, F. R. Chang-DÃŋaz, M. Giambusso, T. W. Glover, A. V. Ilin, J. P. Squire, B. W. Longmier, E. A. Bering, P. A. Cloutier, Investigation of plasma detachment from a magnetic nozzle in the plume of the vx-200 magnetoplasma thruster, IEEE Transactions on Plasma Science 43 (2015) 252–268.

[19] N. Sakaguchi, Y. Kajimura, H. Nakashima, Thrust efficiency calculation for magnetic nozzle in laser fusion rocket, TRANSACTIONS OF THE JAPAN SOCIETY FOR AERONAUTICAL AND SPACE SCIENCES 48 (2005) 180–182.

[20] N. Matsuda, A. Maeno, Y. Kajimura, H. Nakashima, A magnetic thrust chamber design for a laser fusion rocket based on impact fast ignition scheme, Journal of Plasma and Fusion Research SERIES 8 (2009) 1602–1605.

[21] T. D. Arber, K. Bennett, C. S. Brady, A. Lawrence-Douglas, M. G. Ramsay, N. J. Sircombe, P. Gillies, R. G. Evans, H. Schmitz, A. R. Bell, C. P. Ridgers, Contemporary particle-in-cell approach to laser-plasma modelling, Plasma Physics and Controlled Fusion 57 (2015) 113001.

[22] C. K. Birdsall, A. B. Langdon, Plasma Physics via Computer Simulation, Institute of Physics Publishing Bristol and Philadelphia, 1995.

[23] J. Villasenor, O. Buneman, Rigorous charge conservation for local electromagnetic field solvers, Computer Physics Communications 69 (1992) 306–316.

[24] R. Kawabuchi, N. Matsuda, Y. Kajimura, H. Nakashima, Numerical simulation of plasma detachment from a magnetic nozzle by using fully particle-in-cell code, Journal of Physics Conference Series 112 (2008) 042082.

[25] K. V. Vchikov, H. Nakashima, T. Esaki, Y. P. Zakharov, T. Kawano, T. Muranaka, Laser-produced plasma experiments and particle in cell simulation to study thrust conversion processes in a laser fusion rocket, Japanese Journal of Applied Physics 42 (2003) 6590–6597.

[26] B. H. Ripin, J. D. Huba, E. A. McLean, C. K. Manka, T. Peyser, H. R. Burris, J. Grun, Sub-alfvenic plasma expansion, Physics of Fluids B: Plasma Physics 5 (1993) 3491–3506.

[27] Y. Zakharov, Laboratory simulation of artificial plasma releases in space, Advances in Space Research 29 (2002) 1335 – 1344.